IET Renewable Power Generation

Research Article

IET Journals
The Institution of Engineering and Technology

Affinely adjustable robust energy management system for smart homes

ISSN 1752-1416
Received on 11th February 2020
Revised 8th August 2020
Accepted on 14th August 2020
E-First on 18th November 2020
doi: 10.1049/iet-rpg.2020.0186
www.ietdl.org

Cuo Zhang[1] ✉, *Zhao Yang Dong*[1], *Xia Yin*[1]

[1]*School of Electrical Engineering and Telecommunications, The University of New South Wales, Sydney, Australia*

✉ *E-mail: cuo.zhang@unsw.edu.au*

Abstract: As plentiful roof-top photovoltaic (PV) panels and battery energy storage systems (BESSs) have been installed in residential houses, smart homes which provide reliable and cost-efficient energy for customers have been increasingly developing. This study proposes a smart home coordinated operation framework consisting of day-ahead scheduling of a BESS and deferrable appliances as well as real-time BESS affinely adjustable control. The scheduling aims to minimise daily energy usage bills and the affinely adjustable control aims to eliminate fluctuations of intermittent PV output and at-will uncertain appliances. This study proposes an affinely adjustable robust energy management system (AAREMS) which can optimise the day-ahead scheduling with full consideration of the real-time BESS control under uncertainties. Moreover, affinely adjustable robust counterpart formulation is developed to solve the AAREMS under the worst case of real-time uncertainty realisation. The simulation results verify the high efficiency of the proposed AAREMS in minimising the energy usage bills for the customers and providing certain and invariable power injection for the utility grid.

Nomenclature

Sets and indices

I, i	set and index of deferrable loads
J, j	set and index of tasks
T, t	set and index of operation periods
$T(i, j)$	set of preferred operation periods, i.e. preferred operation time range

Parameters

OM	operation and maintenance cost of BESS, \$/kWh
$\mathrm{OT}_{i,j}$	operation time length required by a task, h
P_t^{BL}	baseload demand, kW
p_t^{buy}, p_t^{sell}	price for buying and selling electric energy, \$/kWh
$P_i^{\mathrm{DL,r}}$	deferrable appliance rated power, kW
$P_t^{\mathrm{EX,max}}$	power export limit of smart home, kW
$P_t^{\mathrm{IM,max}}$	power import limit of smart home, kW
η^{ch}, η^{dis}	BESS charging/discharging efficiency, %
η^{sd}	BESS self-discharge rate, %
τ	time length of the operation period, h

Variables

E_t	energy stored in BESS, kWh
P_t^{B}	BESS output power, kW. A positive value for charging, while the negative value for discharging
P_t^{ch}, P_t^{dis}	charging and discharging power of BESS, kW
P_t^{def}, P_t^{sur}	smart home deficient and surplus power, kW
P_t^{SH}	smart home net load demand, power exchange between smart home and utility grid, kW. A positive value for importing power from the grid, while the negative value for exporting power to the grid
P_t^{PV}	photovoltaic power generation, kW
$P_{i,j,t}^{\mathrm{DL}}$	deferrable appliance power consumption, kW
P_t^{UL}	at-will uncertain load demand, kW
SOC_t	state of charge of BESS, %
$\alpha_{i,j,t}$	on/off the binary decision of deferrable appliance task
β_t	slack binary variable of BESS charging/discharging operation state
$\delta_{i,j,t}$	slack binary variable of deferrable appliance task decision

Notation

$()^0$	base value
$()^{\mathrm{l}}$, $()^{\mathrm{u}}$	lower and upper bounds of interval prediction
$()^{\min}$, $()^{\max}$	minimum and maximum limits
$()^{\mathrm{c}}$	capacity
$\Delta()$	uncertain variation
$\overline{()}$	predicted mean value
$\widetilde{()}$	uncertain value

1 Introduction

Roof-top photovoltaic (PV) panels have been proliferating on residential houses, due to improved power generation efficiency and reduced costs. However, the PVs bring challenges such as inverse peak-shaving power generation and severe voltage fluctuations in distribution networks [1].

To tackle the above challenges, applications of smart homes play a vital role in demand-side management. Liu *et al*. [2] defined that smart homes can employ optimal scheduling and automatic control of various household electric appliances in advanced metering infrastructure. Deferrable appliances such as clothe washers and dryers can be optimally scheduled in response to electricity prices or incentive payments to achieve demand response [3]. Thus, the deferrable appliances can provide a potential for efficient load levelling including matching loads to PV power generation. The load levelling achieved by the demand response delivers many benefits such as reducing electricity usage bills for customers [4], deferring capacity upgrade and reducing line losses for utilities [5]. Moreover, the authors in [6] indicate battery energy storage systems (BESSs) can efficiently improve the self-consumption of PV energy to provide a peak shaving potential. Due to continuously decreasing costs, BESSs have been increasingly installed in smart homes to construct a PV-storage system achieving the load levelling [7]. Besides, in [8], BESSs provide an opportunity to deal with intermittent PV power

generation, i.e. smoothing out the PV output power fluctuations which cause severe voltage fluctuations.

With sufficient PV power generation, deferrable appliances and controllable BESSs, the smart home customers have the flexibility of energy management. Yao *et al*. [9] stated that many utilities encourage customers to trade electric energy with the utilities. Thus, a smart home customer becomes a mix of energy producer and consumer, i.e. prosumer. Prosumers need advanced energy management systems (EMSs) to optimise their smart home operation. Wang *et al*. [10] proposed minimisation of electricity usage bills for the customers by scheduling the BESSs considering energy loss due to the rate capacity effect and the power dissipation of conversion circuitry. Different types of loads are optimally scheduled in [11] to minimise the electricity usage bills considering the maximum demand limit (MDL). Furthermore, the work in [12] proposes an EMS to optimally schedule deferrable loads, BESSs and plug-in electric vehicles.

However, the above works [10–12] ignore uncertainties from PV power generation and loads which may impair EMS optimisation results and lead to operating constraint violations. To deal with the uncertainty issue, stochastic programming which models the uncertainties as scenarios is applied in [9] to minimise the electricity usage bills by scheduling deferrable appliances and BESSs. Zhang and Xu [13] applied the scenario-based stochastic optimisation with a probabilistic modelling method to address real-time uncertainty realisation for a voltage/VAR control problem. Additionally, in [14], the robust counterpart is applied to guarantee a robust solution for the smart home EMS optimisation problem under uncertainties. Danandeh *et al*. [15] utilised the two-stage robust optimisation method to model the uncertainties as uncertainty sets when optimising deferrable loads. These methods can alleviate uncertainty's impacts and improve PV energy utilisation efficiency. However, the EMSs for smart homes dispatch deferrable appliances and BESSs in a specific operation period, e.g. 1 h, and they cannot respond in real time to fluctuating and intermittent PV power generation.

On the other hand, autonomous controllers can be embedded in BESSs to achieve smoothing out power fluctuations. Various control strategies are proposed to eliminate PV output power fluctuations, such as ramp-rate control [16], moving average technique [17] and two-stage filter based on digital finite impulse response [18]. With the measured real-time PV power generation, the BESSs can adaptively control charging/discharging power to efficiently eliminate PV output fluctuations. However, the above real-time control methods neglect daily economic dispatch effects, leading to high operating costs for the customers.

From the above literature review, the EMSs and the real-time control methods have, respectively, advantages and disadvantages. They can compensate each other to achieve both the economic benefits and fast response ability. It is sensible to link the scheduling optimisation and real-time control. Wang *et al*. [19] proposed a two-tier operation method of BESSs for smart homes. A global tier minimises monthly bills by formulating BESS charging/discharging schemes while a local tier adaptively controls the BESS output power to ensure the total demand within the MDL. However, uncertainty impacts are not modelled in the global tier and the local tier cannot smooth out fluctuations. More importantly, in this work [19], the EMS and the real-time control are separately designed without coordinated optimisation.

To efficiently tackle the challenges in the literature including the low PV energy utilisation efficiency as well as the uncertain fluctuation of PV power generation and loads, it is necessary to develop an EMS with embedded real-time control for smart homes. In addition, the uncertain PV power generation and loads need to be effectively modelled and addressed in this EMS for smart homes, ensuring operating robustness against the uncertainties. Thus, this paper proposes an affinely adjustable robust EMS (AAREMS) for smart homes which can optimally and robustly coordinate deferrable loads and a BESS embedded with new affinely adjustable control, with full consideration of uncertainties of PV power generation and loads.

Compared with the existing works, this paper makes the following major contributions, in terms of the BESS control model, smart home operation framework and optimisation method to deal with uncertainties.

(i) *An affinely adjustable control model for a BESS* is proposed to address fluctuations of PV power generation and loads. With this control, the BESS can not only shift energy but also act as a 'power buffer'.
(ii) *A smart home coordinated operation framework* considering PV panels, a BESS and various types of loads is proposed. Herein, deferrable load scheduling and the BESS control function are optimised one day ahead and the BESS affinely adjustable control is implemented in real time.
(iii) *An AAREMS* which minimises total operating cost and guarantees operating robustness against any uncertainty realisation is developed. An affinely adjustable robust counterpart (AARC) method is applied to solve the AAREMS problem under the worst case of uncertainty realisation.

The remainder of this paper is organised as follows. Section 2 describes the proposed smart home coordinated operation framework. Section 3 presents the proposed affinely adjustable control model for the BESS. Section 4 formulates models of the BESS, deferrable loads and uncertainties. In Section 5, a smart home EMS model is proposed, and the optimisation problem is solved by the AARC method to achieve an AAREMS under uncertainties. Section 6 carries out numerical simulations of the proposed AAREMS with different tests and demonstrates the results. At last, Section 7 concludes the whole paper and introduces future works.

2 Smart home coordinated operation framework

Smart home with roof-top PV panels, a BESS and various electric appliances can be regarded as a nano generation–storage–load hybrid energy system.

PV panels generate clean and cost-effective power to the smart home. However, the PV output power is uncertain and intermittent, impairing smart home operation. The medium-term PV power generation can be predicted within intervals and the interval predictions can help more efficiently present uncertainty characteristics for the operation optimisation of the smart home.

A BESS can achieve an energy-shifting function by storing low cost or surplus renewable energy in off-peak periods and releasing it in peak periods to match peak loads. This function can provide economic and technical benefits such as reduced electricity usage bills for customers and load levelling for utilities. On the other hand, the BESS can respond to varying PV power generation and loads in real time, smoothing out power fluctuations. As a result, the power exchange (generation and consumption) between the smart home and the utility grid can be certain and invariable. To simultaneously reduce the customer bills and eliminate the fluctuations, the BESS control function must be robustly optimised under the uncertainties.

Residential loads, i.e. electric appliances, can be classified into three categories: base loads, deferrable loads and at-will uncertain loads. The base loads including refrigerators are essential to work all day. The deferrable loads such as cooking appliances, clothe washers and dryers can be optimally scheduled in respective preferred operation time ranges. The at-will uncertain loads such as computers, TVs and space heaters can be turned on/off at customers' will without concerning usage costs.

Considering the above smart home components and their characteristics, this paper proposes a coordinated operation framework consisting of day-ahead scheduling and real-time control. The proposed framework is demonstrated in Fig. 1 where magenta lines indicate prediction data, red lines indicate real-time measurement and blue lines indicate decision/control signals.

There are two operation stages, i.e. day-ahead scheduling stage and real-time control stage.

In the day-ahead scheduling stage, first, 24-h interval predictions of the uncertainties including expected values as well as lower and upper bounds are obtained. Second, with the interval predictions, an AAREMS optimiser optimises deferrable load

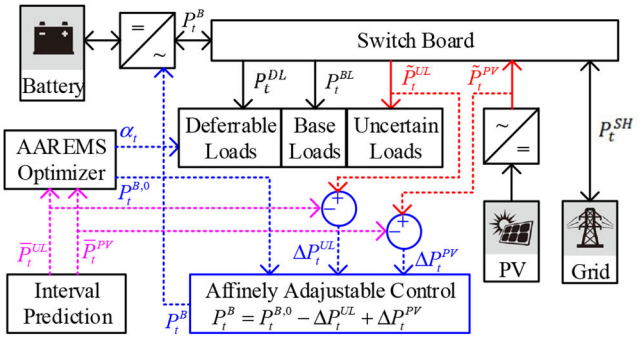

Fig. 1 *Smart home coordinated operation framework*

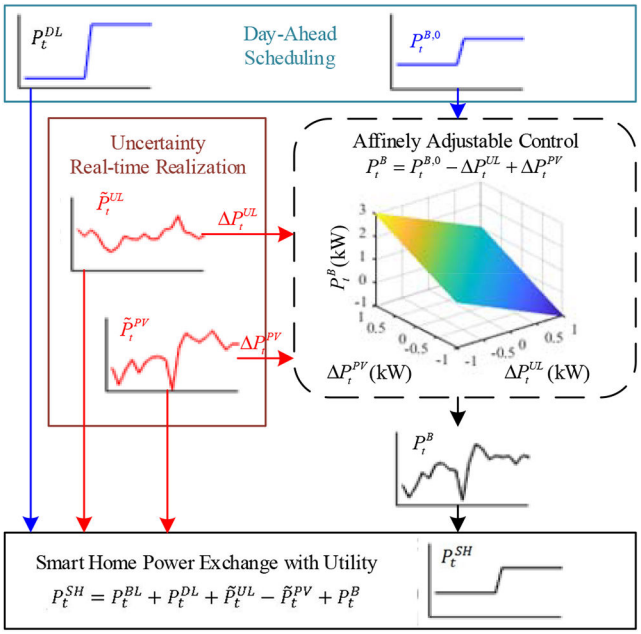

Fig. 2 *Affinely adjustable control*

scheduling and a BESS affine control function. The AAREMS optimiser aims to robustly minimise the total operating cost for the customers with full consideration of the real-time uncertainties. Development of the AAREMS is presented in detail in Section 5. The scheduled deferrable loads and the optimal BESS control function are implemented at a specific operation time interval (e.g. 5 or 30 min) in the following day.

In the real-time control stage, real-time PV output power $\tilde{P}_t^{\mathrm{PV}}$ and at-will uncertain loads $\tilde{P}_t^{\mathrm{UL}}$ can be measured by the PV inverter and the smart meter. Accordingly, real-time variations can be calculated as the real-time measurement values minus the day-ahead expected values. Then, according to the optimised BESS control function, the affinely adjustable control computes the required real-time BESS output power as a setpoint signal. Immediately, the computed setpoint signal is sent to the BESS inverter to control the output power. The affinely adjustable control is introduced in Section 3.

In this framework, the day-ahead deferrable load scheduling and the BESS control function used in real time are simultaneously optimised by the AAREMS optimiser with full consideration of the real-time uncertainties. Thus, the day-ahead scheduling stage and the real-time control stage can be efficiently and robustly coordinated.

It is worth noting that the AAREMS optimiser can be a central optimiser for multiple smart homes. The residential load information and the renewable power generation prediction of each home can be collected in the central AAREMS optimiser through remote communications, such as enhanced machine-type communication. Then, the central AAREMS optimiser optimises the deferrable load scheduling and the BESS control function for each home and dispatches the optimal solution to each home via the remote communications. Additionally, note that distribution network operating conditions can be modelled as constraints in the central AAREMS optimiser, such that impacts of the smart homes on the distribution network can be considered. However, consideration of the distribution network does not affect the effectiveness of the proposed smart home coordinated operation framework.

3 BESS as 'power buffer'

A BESS with an embedded autonomous controller can adaptively control its charging/discharging power according to real-time fluctuations of PV power generation and load demand. Through the adaptive control of the BESS output power, the real-time fluctuations of PV power generation and load demand can be eliminated. Thus, the BESS can act as a 'power buffer' to highly frequently and fast store surplus power and release it to compensate for power deficiency.

To achieve certain and invariable power exchange between the smart home and the utility, the BESS is expected to eliminate fluctuations of net load demand, i.e. total loads minus PV power generation. Thus, the BESS output power is controlled to compensate the net load demand fluctuations as

$$P_t^{\mathrm{B}} = P_t^{\mathrm{B},0} - \Delta P_t^{\mathrm{SH}}, \quad \forall t. \tag{1}$$

For the smart home, the fluctuations of the PV output power and the at-will uncertain loads cause the net load demand fluctuations, with the following relationship:

$$\Delta P_t^{\mathrm{SH}} = \Delta P_t^{\mathrm{UL}} - \Delta P_t^{\mathrm{PV}}, \quad \forall t. \tag{2}$$

Substitute (2) into (1), the BESS output power can be reformulated as the following affine function:

$$P_t^{\mathrm{B}} = P_t^{\mathrm{B},0} - \Delta P_t^{\mathrm{UL}} + \Delta P_t^{\mathrm{PV}}, \quad \forall t. \tag{3}$$

The autonomous controller in the BESS can employ the affine function (3) to achieve an affinely adjustable control model of the BESS output power. This control strategy is demonstrated in Fig. 2. In the day-ahead scheduling stage, the BESS base output power set-point is optimised, and it is used to construct the affine function (3). In the real-time control stage, the PV output power and the at-will uncertain loads are measured in real time and the corresponding fluctuations are calculated. Then, these real-time fluctuations are used as the inputs of (3) in the autonomous controller and the controller adjusts the BESS output power P_t^{B} according to (3). Note that the real-time BESS output power is adaptively controlled around the optimised base output power, such that the day-ahead optimal scheduling still takes effect. As a result, the net load demand, also as the power exchange between the smart home and the utility grid, is controlled as a certain and invariable value without any fluctuation. The real-time power exchange would be exactly the same with the day-ahead optimised power exchange, such that the utility can optimise the power system operation without being impacted by the uncertainty of residential loads.

It is worth noting that this affinely adjustable control model is based on a linear decision rule and it is a tractable model which can be flexibly applied in the advanced optimisation methods.

In practice, the BESS adaptive control with the affine function (3) can be embedded and updated in the inverter. Via short-range communications between the local smart home EMS and the inverter, the optimised affine function is updated in the inverter at the same short time interval in coordination with deferrable appliance tasks. The PV power generation and the load power consumption are measured by the smart meters in real time. Then, the BESS inverter responds to measured fluctuations of the PV power generation and the loads, and it automatically adjusts its output power according to the embedded affine function (3). Here, the BESS real-time control based on the affine function (3) can be

implemented through fast-responsive control methods in power electronics development [20].

4 Mathematical models

This paper proposes a mathematical optimisation model for smart home EMS. The mathematical models of the BESS, the deferrable loads and the uncertainty impacts are developed in this section.

4.1 BESS model

Practical BESS operating concerns such as power capacity, energy storage efficiency and dynamics must be modelled.

The BESS output power is limited within the capacity as

$$-P^{\mathrm{dis,c}} \le P_t^{\mathrm{B}} \le P^{\mathrm{ch,c}}, \quad \forall t. \tag{4}$$

To efficiently model the BESS dynamic operation, P_t^{ch} and P_t^{dis} are introduced to express the BESS dynamic charging/discharging power. They have the following limits:

$$0 \le P_t^{\mathrm{ch}} \le P^{\mathrm{ch,c}}, \quad \forall t, \tag{5a}$$

$$0 \le P_t^{\mathrm{dis}} \le P^{\mathrm{dis,c}}, \quad \forall t, \tag{5b}$$

$$P_t^{\mathrm{ch}} P_t^{\mathrm{dis}} = 0, \quad \forall t. \tag{5c}$$

To linearise the non-linear constraint (5c), a slack binary variable β_t is utilised to indicate the BESS charging ($\beta_t = 1$) and discharging ($\beta_t = 0$) operation and the constraint (5a)–(5c) can be reformulated into a linear equivalent constraint as

$$0 \le P_t^{\mathrm{ch}} \le \beta_t P^{\mathrm{ch,c}}, \quad \forall t, \tag{6a}$$

$$0 \le P_t^{\mathrm{dis}} \le (1-\beta_t) P^{\mathrm{dis,c}}, \quad \forall t. \tag{6b}$$

Moreover, the BESS dynamic output power P_t^{B} has the following relationship with P_t^{ch} and P_t^{dis}:

$$P_t^{\mathrm{B}} = P_t^{\mathrm{ch}} - P_t^{\mathrm{dis}}, \quad \forall t. \tag{7}$$

P_t^{ch} and P_t^{dis} are also applied to calculate the BESS operation and maintenance (O&M) cost. For a minimisation problem of the BESS O&M cost, P_t^{ch} and P_t^{dis} are expected to be optimised as the smallest values while satisfying the constraints. Thus, (7) can be reformulated as two inequality constraints as

$$P_t^{\mathrm{ch}} \ge P_t^{\mathrm{B}}, \quad \forall t, \tag{8}$$

$$P_t^{\mathrm{dis}} \ge -P_t^{\mathrm{B}}, \quad \forall t, \tag{9}$$

Considering the self-discharge rate and inverter efficiency, the BESS dynamic energy storage is modelled according to the dynamic charging/discharging power as

$$E_t = \left(1-\eta^{\mathrm{sd}}\right) E_{t-1} + \eta^{\mathrm{ch}} P_t^{\mathrm{ch}} \tau - P_t^{\mathrm{dis}} \tau / \eta^{\mathrm{dis}}, \quad \forall t. \tag{10}$$

Accordingly, the dynamic state of charge (SOC) of the BESS is calculated and limited within an allowed range as

$$\mathrm{SOC}_t = E_t / E^{\mathrm{c}}, \quad \forall t, \tag{11}$$

$$\mathrm{SOC}_t^{\min} \le \mathrm{SOC}_t \le \mathrm{SOC}_t^{\max}, \quad \forall t. \tag{12}$$

The BESS dynamic operation model with the practical limits formed by (4), (6a), (6b), (8)–(12) is a tractable linear model, which is fully compatible to advanced optimisation methods such as robust optimisation.

4.2 Deferrable load model

A smart home usually has a variety of deferrable loads which customers can use for different household tasks during a day. To efficiently schedule the deferrable loads, the customers need to set appliance and task parameters including a preferred operation time range and an operation time length for each task. These parameters can also be obtained from questionnaires to a representative sample of customers [21]. This paper assumes that the customers would be satisfied if the appliances work in the corresponding preferred operation time ranges. Given these parameters, a specific appliance can be optimally allocated within the preferred operation time range to work for the fixed operation time length. By doing so, customers' preferences and task requirements can be considered in the day-ahead scheduling.

First, a binary variable $\alpha_{i,j,t}$ is introduced to determine whether a task j of a deferrable appliance i is scheduled in the operation period t. Thus, the power consumption of a deferrable appliance is modelled as

$$P_{i,j,t}^{\mathrm{DL}} = \alpha_{i,j,t} P_i^{\mathrm{DL,r}}, \quad \forall i, j, t. \tag{13}$$

When a task is scheduled, the appliance would be kept on until the task is completed without any interrupt. This characteristic is modelled as:

$$\sum_{t \in T(i,j)} \alpha_{i,j,t} = \mathrm{OT}_{i,j}, \quad \forall i, j. \tag{14}$$

$$\sum_{t \in T(i,j)} \left|\alpha_{i,j,t} - \alpha_{i,j,t-1}\right| \le 2, \quad \forall i, j. \tag{15}$$

Constraint (15) is non-linear due to the absolute value form. A slack binary variable $\delta_{i,j,t}$ is utilised to eliminate the non-linearity of (15) as

$$\delta_{i,j,t} \ge \alpha_{i,j,t} - \alpha_{i,j,t-1}, \quad \forall i, j, t, \tag{16a}$$

$$\delta_{i,j,t} \ge \alpha_{i,j,t-1} - \alpha_{i,j,t}, \quad \forall i, j, t, \tag{16b}$$

$$\sum_{t \in T(i,j)} \delta_{i,j,t} \le 2, \quad \forall i, j. \tag{16c}$$

In the condition that $\alpha_{i,j,t} > \alpha_{i,j,t-1}$, (16a) works to provide a reduced feasible region as $\delta_{i,j,t} \ge 1$ but (16b) becomes ineffective. On the other hand, in the condition that $\alpha_{i,j,t} < \alpha_{i,j,t-1}$, (16b) works but (16a) does not. If $\alpha_{i,j,t} = \alpha_{i,j,t-1}$, (16a) and (16b) become same as $\delta_{i,j,t} \ge 0$. Thus, only if (16a) and (16b) are used together, the absolute calculation for the left side of inequality constraint (15) can be relaxed.

Moreover, when a task is scheduled, the other tasks of the same appliance cannot be scheduled. Thus, for a specific appliance, on/off decisions of different tasks are constrained as

$$\sum_{j \in J} \alpha_{i,j,t} \le 1, \quad \forall i, t. \tag{17}$$

In practice, smart plugs are utilised to switch on and off the scheduled appliances. According to the day-ahead scheduling decision, the smart plugs are controlled by the local smart home EMS via short-range communications [22].

It is worth noting that the base loads and the at-will uncertain loads must also be modelled in the EMS. The base loads are modelled as constant power consumption. The at-will uncertain loads are modelled as uncertainty variables which vary randomly within the predicted intervals. If thermal at-will uncertain appliances such as space heaters are considered, the user thermal comfort model and the building thermal model are required [23]. However, thermal models do not affect the effectiveness of the proposed smart home EMS.

4.3 Uncertainty impacts on power systems

PV power generation and at-will uncertain loads randomly vary in real time. They can significantly impair both the day-ahead scheduling and real-time control, leading to increased operating costs and operating constraint violation. Therefore, their impacts are required to be modelled and addressed.

Generally, the real-time uncertainties vary around expected values which can be predicted. Thus, a real-time uncertainty variable can be modelled as summation of the predicted value and the real-time uncertain variation. The varying PV power generation and uncertain loads are modelled as

$$\tilde{P}_t^{\mathrm{PV}} = \bar{P}_t^{\mathrm{PV}} + \Delta P_t^{\mathrm{PV}}, \quad \forall t, \tag{18}$$

$$\tilde{P}_t^{\mathrm{UL}} = \bar{P}_t^{\mathrm{UL}} + \Delta P_t^{\mathrm{UL}}, \quad \forall t\,. \tag{19}$$

With the varying PV power generation and uncertain loads, the impacted real-time net load demand (power exchange between the smart home and the utility grid) is computed and it must be kept within the MDL [11] as:

$$P_t^{\mathrm{SH}} = P_t^{\mathrm{BL}} + \sum_{i \in I} \sum_{j \in J} P_{i,j,t}^{\mathrm{DL}} + \tilde{P}_t^{\mathrm{UL}} + P_t^{B} - \tilde{P}_t^{\mathrm{PV}}, \quad \forall t, \tag{20}$$

$$-P_t^{\mathrm{EX,max}} \le P_t^{\mathrm{SH}} \le P_t^{\mathrm{IM,max}}, \quad \forall t\,. \tag{21}$$

Here P_t^{BL}, $P_{i,j,t}^{\mathrm{DL}}$, $\tilde{P}_t^{\mathrm{UL}}$ and $\tilde{P}_t^{\mathrm{PV}}$ are positive parameters or variables. $\tilde{P}_t^{\mathrm{PV}}$ is given the '−' sign to indicate power generation, while others denote loads. The smart home imports power from the grid if P_t^{SH} is positive, while it exports power to the grid if P_t^{SH} is negative. The BESS charges power if P_t^{B} is positive, while it discharges power if P_t^{B} is negative.

5 Affinely adjustable robust EMS

Based on the proposed smart home coordinated operation framework, an AAREMS which can both minimise the total operating cost and guarantee the operating constraint satisfaction under the uncertainties is developed in this section.

5.1 EMS for smart homes

The EMS for smart homes aims to minimise the total operating cost for the customers consisting of the BESS O&M cost and the electricity usage bill.

The BESS O&M cost over a day is calculated according to charged and discharged energy as

$$C^{\mathrm{BESS}} = \sum_{t \in T} \mathrm{OM}\left(P_t^{\mathrm{ch}} + P_t^{\mathrm{dis}}\right)\tau\,. \tag{22}$$

As the prosumers in the power systems, the customers can sell surplus energy to obtain a payback. Thus, the electricity usage bill is calculated as subtracting the payback from the energy usage payment. To efficiently calculate the usage bill, two slack variables, P_t^{def} and P_t^{sur}, are introduced to present deficient and surplus power. They have the following constraints:

$$P_t^{\mathrm{SH}} = P_t^{\mathrm{def}} - P_t^{\mathrm{sur}}, \quad \forall t, \tag{23a}$$

$$P_t^{\mathrm{def}} \ge 0, \quad \forall t, \tag{23b}$$

$$P_t^{\mathrm{sur}} \ge 0, \quad \forall t\,. \tag{23c}$$

If $P_t^{\mathrm{def}} > 0$, it means the smart home prosumers buy electric energy from the utility; if $P_t^{\mathrm{sur}} > 0$, it means the prosumers sell surplus energy to the utility.

With (23a)–(23c), the electricity usage bill is computed as

$$C^{\mathrm{EB}} = \sum_{t \in T} p_t^{\mathrm{buy}} P_t^{\mathrm{def}} \tau - p_t^{\mathrm{sell}} P_t^{\mathrm{sur}} \tau\,. \tag{24}$$

The EMS optimisation problem is modelled as

$$\begin{aligned} &\min\ C^{\mathrm{BESS}} + C^{\mathrm{EB}} \\ &\text{s.t.}\ \ (3), (4), (6a), (6b), (8)-(14), (16a)-(16c), (17)-(24) \end{aligned} \tag{25}$$

The EMS optimisation problem is mixed-integer linear programming. The control variables include the deferrable load scheduling decision $\alpha_{i,j,t}$, and the BESS base output power $P_t^{\mathrm{B},0}$. The uncertainty variables include the variation of the PV power generation ΔP_t^{PV} and the variation of the at-will uncertain loads ΔP_t^{UL}.

5.2 Uncertainty set modelling

To guarantee the real-time operating robustness, the real-time uncertainty realisation is required to be considered in the proposed EMS. Interval uncertainty sets constructed by lower and upper bounds can provide continuous uncertainty variables, so that they can fully cover all the possible uncertainty realisation, more accurately than discrete samples. Therefore, in this paper, the uncertain PV power generation and the uncertain loads are modelled as the following interval uncertainty sets as

$$\tilde{P}_t^{\mathrm{PV}} \in \left[P_t^{\mathrm{PV,l}}, P_t^{\mathrm{PV,u}}\right], \quad \forall t, \tag{26}$$

$$\tilde{P}_t^{\mathrm{UL}} \in \left[P_t^{\mathrm{UL,l}}, P_t^{\mathrm{UL,u}}\right], \quad \forall t\,. \tag{27}$$

Herein, the lower and upper bounds of the sets can be obtained by interval prediction techniques [24]. With the predicted mean values of the uncertainty variables $\bar{P}_t^{\mathrm{PV}}$ and $\bar{P}_t^{\mathrm{UL}}$, the real-time uncertain variations can be further modelled as

$$\Delta P_t^{\mathrm{PV}} \in \left[P_t^{\mathrm{PV,l}} - \bar{P}_t^{\mathrm{PV}}, P_t^{\mathrm{PV,u}} - \bar{P}_t^{\mathrm{PV}}\right], \quad \forall t, \tag{28}$$

$$\Delta P_t^{\mathrm{UL}} \in \left[P_t^{\mathrm{UL,l}} - \bar{P}_t^{\mathrm{UL}}, P_t^{\mathrm{UL,u}} - \bar{P}_t^{\mathrm{UL}}\right], \quad \forall t\,. \tag{29}$$

The uncertainty sets (28) and (29) are added as constraints in the proposed EMS model (25) to express the real-time uncertain variations. The uncertainty sets can provide the worst case of all the possible uncertainty realisation which is used in the robust optimisation to obtain a robust solution against any uncertainty realisation. Uncertainty budgets can be considered to reduce solution conservativeness which may be caused by the robust optimisation [25].

5.3 Compact reformulation

With the above uncertainty modelling, the proposed EMS model can be reformulated into a compact matrix form as follows:

$$\min_{\boldsymbol{x},\,\boldsymbol{y}} \ \boldsymbol{a}^{\mathrm{T}}\boldsymbol{x} \tag{30}$$

$$\text{s.t.} \quad \boldsymbol{y} = \boldsymbol{C}\boldsymbol{x} + \boldsymbol{D}\boldsymbol{u} \tag{31}$$

$$\boldsymbol{A}\boldsymbol{x} \le \boldsymbol{b} \tag{32}$$

$$\boldsymbol{A}_{\mathrm{eq}}\boldsymbol{x} = \boldsymbol{b}_{\mathrm{eq}} \tag{33}$$

$$\boldsymbol{E}\boldsymbol{x} + \boldsymbol{F}\boldsymbol{y} + \boldsymbol{G}\boldsymbol{u} \le \boldsymbol{h} \tag{34}$$

$$\boldsymbol{u} \in \left[\boldsymbol{u}^{\mathrm{l}}, \boldsymbol{u}^{\mathrm{u}}\right] \tag{35}$$

Here $\boldsymbol{x}$ presents the vector of the control variables ($\alpha_{i,j,t}$ and $P_t^{\mathrm{B},0}$), dependent variables (P_t^{ch}, P_t^{dis}, P_t^{def}, P_t^{sur}, E_t and SOC_t) and slack variables (β_t and $\delta_{i,j,t}$); $\boldsymbol{y}$ presents the vector of the affinely

adjustable variables (P_t^{B}) and $\boldsymbol{u}$ presents the vector of the uncertainty variables (ΔP_t^{PV} ΔP_t^{UL}). Besides, bold-italic uppercase letters express matrices of parameters and bold-italic lowercase letters express vectors of parameters. Description of formulating this compact matrix model can be found in the Appendix.

5.4 Affinely adjustable robust counterpart

To fully address the uncertainties of the PV power generation and the at-will loads, robust optimisation techniques [26] which optimise problems under the worst case of uncertainty realisation can guarantee a feasible solution under uncertainties. In addition, compared with the stochastic optimisation, the robust optimisation does not require probability distribution data and it can achieve high-computing efficiency [27]. Considering the above advantages, the robust optimisation techniques have been widely applied in power system problems, such as unit commitment [27] and multi-energy microgrid operation [25]. For the EMS problems, the robust optimisation techniques can achieve robust operation against any uncertainty realisation, i.e. no operating constraint violation occurs.

For tractable optimisation problems such as linear programming problems, the work [26] proposes AARC formulation to optimise parameters of affine functions with full consideration of uncertainty realisation. The AARC method is one type of robust optimisation and it can achieve high computing efficiency without requiring probability distribution data. More importantly, the AARC method solves the optimisation problems under the worst case of uncertainty realisation, guaranteeing robust solutions. Since the proposed EMS is a tractable linear model with the affine function (3), this paper applies an AARC to optimise the deferrable load scheduling $\alpha_{i,j,t}$ and the BESS base output power $P_t^{\mathrm{B},0}$, considering the uncertainty variables ΔP_t^{PV} and ΔP_t^{UL}. As a result, for any real-time uncertainty realisation, a feasible solution, i.e. feasible BESS output power P_t^{B} can be obtained while all the operating constraints are satisfied. It means that robust operation against any real-time uncertainty realisation can be guaranteed.

The proposed AARC modelling is derived based on the compact EMS model formulated in Section 5.3. First, the affine function (31) is substituted into (34)

$$(\boldsymbol{E}+\boldsymbol{FC})\boldsymbol{x}+(\boldsymbol{G}+\boldsymbol{FD})\boldsymbol{u}\le\boldsymbol{h}. \tag{36}$$

Considering the uncertainty set (35), the solution feasibility can be guaranteed by

$$(\boldsymbol{E}+\boldsymbol{FC})\boldsymbol{x}+\max_{\boldsymbol{u}\in[\boldsymbol{u}^{\mathrm{l}},\boldsymbol{u}^{\mathrm{u}}]}(\boldsymbol{G}+\boldsymbol{FD})\boldsymbol{u}\le\boldsymbol{h}. \tag{37}$$

Here the maximisation term in (37) aims to search for the worst case of uncertainty realisation which still satisfies constraint (37). In other words, if the worst case of uncertainty realisation can satisfy constraint (36), any other uncertainty realisation can satisfy (36) as well. Thus, the optimisation solution obtained under the worst case is robust against any uncertainty realisation.

To effectively present the worst case in the optimisation model, constraint (37) is expected to be transformed into linear constraints. For the mth constraint of (37) and the nth uncertainty variable u_n, the maximisation term in (37) can be transformed into two linear functions with conditions as

$$\forall m,n:\ \max_{u_n\in[u_n^{\mathrm{l}},u_n^{\mathrm{u}}]}(\boldsymbol{G}+\boldsymbol{FD})_{mn}u_n=\begin{cases}(\boldsymbol{G}+\boldsymbol{FD})_{mn}u_n^{\mathrm{u}}, & \text{if } (\boldsymbol{G}+\boldsymbol{FD})_{mn}\ge 0\\ (\boldsymbol{G}+\boldsymbol{FD})_{mn}u_n^{\mathrm{l}}, & \text{if } (\boldsymbol{G}+\boldsymbol{FD})_{mn}<0\end{cases}. \tag{38}$$

To express the conditions in an efficient mathematical model, two slack variables φ_{mn}^{-} and φ_{mn}^{+} are utilised to transform the mth constraint of (37) into linear constraints as

$$\forall m:\ (\boldsymbol{E}+\boldsymbol{FC})_m\boldsymbol{x}+\sum_n\left(\varphi_{mn}^{+}u_n^{\mathrm{u}}+\varphi_{mn}^{-}u_n^{\mathrm{l}}\right)\le h_m, \tag{39a}$$

$$\forall m,n:\ \varphi_{mn}^{+}\ge 0,\quad \varphi_{mn}^{+}\ge(\boldsymbol{G}+\boldsymbol{FD})_{mn}, \tag{39b}$$

$$\forall m,n:\ \varphi_{mn}^{-}\le 0,\quad \varphi_{mn}^{-}\le(\boldsymbol{G}+\boldsymbol{FD})_{mn}. \tag{39c}$$

Thus, the AARC of the original EMS compact model (30)–(35) is formulated as

$$\min_{\boldsymbol{x},\boldsymbol{\theta}^{+},\boldsymbol{\theta}^{-}}\ \boldsymbol{a}^{\mathrm{T}}\boldsymbol{x} \tag{40}$$

$$\text{s.t. } \boldsymbol{A}\boldsymbol{x}\le\boldsymbol{b} \tag{41}$$

$$\boldsymbol{A}_{\mathrm{eq}}x=\boldsymbol{b}_{\mathrm{eq}} \tag{42}$$

$$(\boldsymbol{E}+\boldsymbol{FC})x+\boldsymbol{\theta}^{+}\boldsymbol{u}^{\mathrm{u}}+\boldsymbol{\theta}^{-}\boldsymbol{u}^{\mathrm{l}}\le\boldsymbol{h} \tag{43}$$

$$\begin{aligned}&\boldsymbol{\theta}^{+}\ge 0,\quad \boldsymbol{\theta}^{+}\ge(\boldsymbol{G}+\boldsymbol{FD}),\\ &\boldsymbol{\theta}^{-}\le 0,\quad \boldsymbol{\theta}^{-}\le(\boldsymbol{G}+\boldsymbol{FD})\end{aligned} \tag{44}$$

Here $\boldsymbol{\theta}^{+}$ and $\boldsymbol{\theta}^{-}$ indicate the matrices of the slack variables φ_{mn}^{-} and φ_{mn}^{+}.

The AARC model is still a mixed-integer linear programming problem and it can be directly solved by commercial solvers such as GUROBI solver [28].

With the AARC to solve the proposed EMS problem, the affinely adjustable control of the BESS can be robustly enabled for the smart homes under the uncertainties. Thus, the total operating cost is minimised while the real-time operation is robust against any uncertainty realisation, such that an AAREMS can be achieved.

6 Numerical simulation

6.1 Test system description

The smart home has a BESS with power capacity ($P^{\mathrm{B,c}}$) of 5 kW, energy storage capacity (E^{c}) of 13.5 kWh, inverter efficiency ($\eta^{\mathrm{ch/dis}}$) of 95% and self-discharge rate (η^{sd}) of 0.006% per half an hour (based on 8% per month under the condition of 30°C, 100% SOC and 0 capacity fade [29]). Base loads (P_t^{BL}) are 1 kW, at-will uncertain loads can be up to 2 kW ($P_t^{\mathrm{UL,u}}$) and deferrable load parameters are given in Table 1. The time-of-use electricity price for the customers is shown in Fig. 3. The price for selling surplus electric energy to the utility is 30% of the electricity price for the customers. Day-ahead interval predictions of the roof-top PV power generation for a sunny day and a cloudy day, respectively, is demonstrated in Fig. 4. The limit of power exported from the smart home to the utility grid ($P_t^{\mathrm{EX,max}}$) is 5 kW. The operation time

Table 1 Deferrable load parameters

Deferrable load	Preferred operation time range	Average power, kW	Operation time length, h	Task number
clothes washer	8:00–14:00	0.5	1	2
clothes dryer	11:00–17:00	2.0	1	1
dish washer	14:00–18:00	1.5	2	1
iron	5:00–7:00	1.0	1	1
vacuum cleaner	9:00–21:00	0.4	0.5	2
microwave oven	11:00–14:00	1.2	0.5	1
	15:00–18:00	1.2	0.5	3
rice cooker	14:00–17:00	0.2	1	1
kettle	5:00–8:00	1.2	0.5	1
toaster	5:00–8:00	0.8	0.5	1

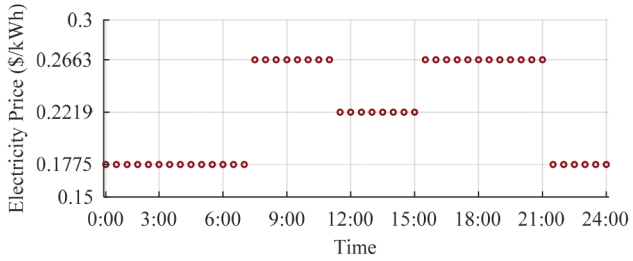

Fig. 3 *Time-of-use electricity price for customers*

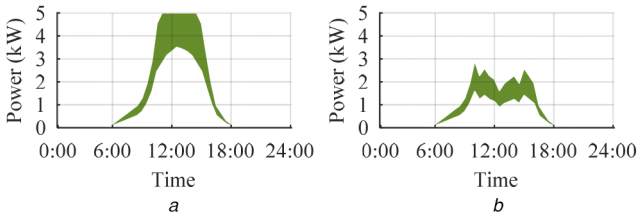

Fig. 4 *Interval prediction of PV power generation*
(a) Sunny day, ***(b)*** Cloudy day

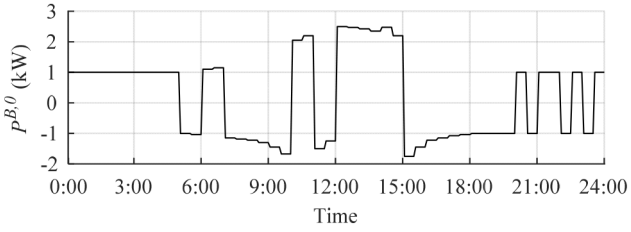

Fig. 5 *BESS base output power*

Table 2 Optimally scheduled deferrable loads

Deferrable load	Operation time	Deferrable load	Operation time
clothes washer	9:00–10:00	microwave oven	11:00–11:30
	11:00–12:00		15:00–15:30
clothes dryer	11:00–12:00		15:30–16:00
dishwasher	15:00–17:00		16:00–16:30
iron	5:00–6:00	rice cooker	14:00–15:00
vacuum cleaner	9:00–9:30	kettle	5:00–5:30
	11:30–12:00	toaster	5:00–5:30

interval used for BESS affine function update is set as 30 min, which is the minimum time interval of deferrable load tasks. Note that other parameter settings (BESS capacity and efficiency, deferrable loads and tasks, electricity prices, prediction data as well as operation time interval) can also be used without affecting the simulation effectiveness.

The simulation is conducted on a 64-bit PC with dual 3.40 GHz CPU and 16.0 GB RAM using MATLAB platform and YALMIP interface [30]. The proposed AAREMS problem is solved by GUROBI solver [28].

6.2 Simulation results of sunny day case

6.2.1 Day-ahead scheduling decisions: With the day-ahead electricity price and PV power generation prediction for the sunny day, the AAREMS problem (40)–(44) is solved by GUROBI solver. The objective i.e. the total operating cost under the worst case is minimised as $11.7171. Note that the actual total operating cost can be further minimised if the worst case does not occur.

The BESS base output power for the affinely adjustable control is optimised and shown in Fig. 5. The BESS SOC under the worst case is illustrated in Fig. 6.

The BESS charges power to store low-cost energy from the utility grid during the off-peak period (0:00–7:00) except when some deferrable loads are used. The BESS also stores energy when

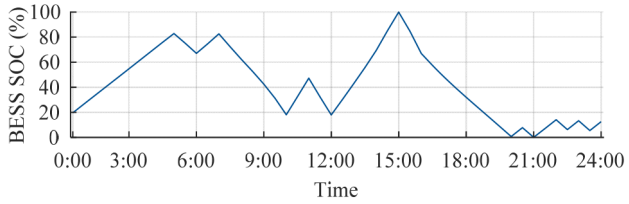

Fig. 6 *BESS SOC under the worst case*

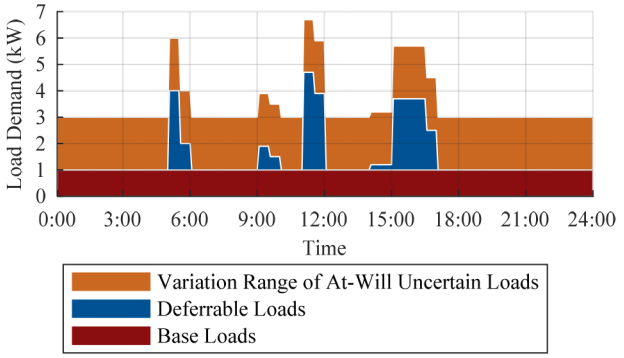

Fig. 7 *Load demand with scheduled deferrable loads*

the PV power generation is surplus (12:00–15:00). On the other hand, the BESS discharges power to fulfill the loads locally during the peak period after 15:00 until the storage is empty at 20:00. In addition, the BESS discharges power slightly during the evening off-peak period for the daily operation reserve requirement.

With the optimised BESS base output power, the BESS affinely adjustable control function is optimally determined, and it is expected to keep the net load demand certain and invariable. Thus, the real-time net load demand will be the same as the day-ahead scheduling result through the real-time affinely adjustable control on the BESS output power.

It is worth noting that the BESS SOC results in Fig. 6 where the SOC reaches the maximum and minimum limits for the worst case of uncertainty realisation, which indicates the extreme SOC of all possible cases of uncertainty realisation. Thus, the BESS energy capacity is sufficient for the worst case, such that it is also sufficient for other uncertainty realisation cases.

In addition, the optimised schedule of the deferrable loads is shown in Table 2 and the 24-h power consumption of the different loads is shown in Fig. 7.

Overall, according to the preferred operation time ranges, the deferrable loads are scheduled into the off-peak period or the high PV power generation period as much as possible. It is worth noting that for saving the usage bill, the appliances which are required to work in the morning, i.e. iron, kettle and toaster, are scheduled before the electricity price goes up to the peak. In addition, after the BESS is fully charged at 15:00, the evening appliances such as a microwave oven and dishwasher are scheduled to work as early as possible to consume the PV power generation.

In terms of computing efficiency, the solver time is 8.3824 s, which is fully compatible with practical on-line use.

6.2.2 Real-time BESS affinely adjustable control: With the optimised day-ahead scheduling of the BESS base output power, the BESS affinely adjustable control is implemented in real time in the following day. To check the performance of the BESS affinely adjustable control, first, uncertain and varying PV power generation and at-will loads are sampled for each 5-min time point and they are shown in Fig. 8. They are regarded as the uncertainty realisation in real time in the smart home coordinated operation model. Second, the real-time variations are calculated by the realisation values minus the mean values from the day-ahead prediction. Then, according to the optimised affinely adjustable control function (3), the autonomous controller adjusts the BESS output power with the real-time variations of the PV power generation and the at-will loads as the inputs. The output is the real-time responding BESS output power P_t^{B} which is demonstrated

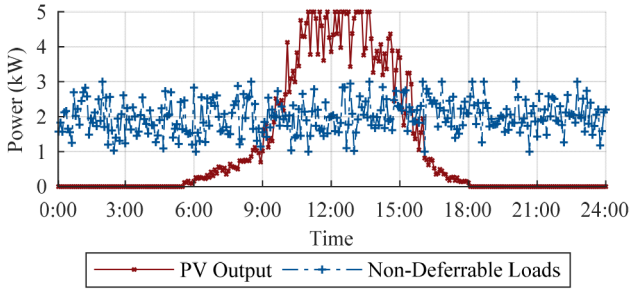

Fig. 8 *Uncertainty realisation*

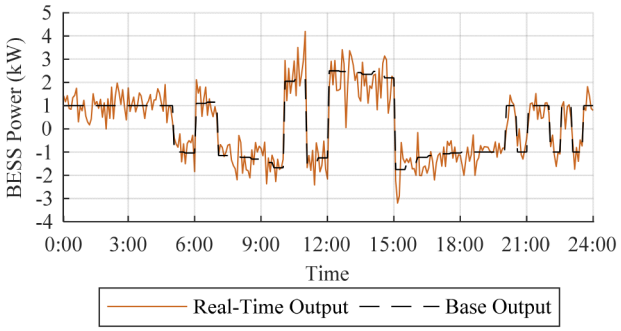

Fig. 9 *Real-time BESS output power*

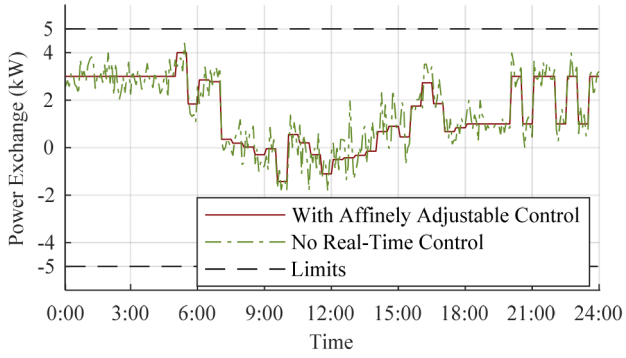

Fig. 10 *Power exchange between smart home and grid*

in Fig. 9. Following the optimised affinely adjustable control function, the real-time BESS output power is controlled to vary around the base output power, indicating the BESS can respond in real time and track the fluctuating PV output power and at-will loads.

The power exchange between the smart home and the utility grid is shown in Fig. 10. The green dashed line indicates that the power exchange would fluctuate significantly with the fluctuations of the PV power generation and at-will loads, if the real-time affinely adjustable control is not applied, as the existing work [12]. In comparison, with the AAREMS and the affinely adjustable control, the real-time responding BESS output power can fully compensate the fluctuations of the PV output power and the at-will loads such that the power exchange is flat without any fluctuation for each operation period (30 min). More importantly, the power exchange is kept certain as the optimised one in the day-ahead scheduling. The utility can benefit from this certain and invariable power exchange, due to no residential load demand uncertainty or fluctuation issue to the utility level operation. Moreover, the real-time power exchange is kept within the allowed limits, indicating no operating constraint violation issue.

6.2.3 Monte Carlo feasibility check: To comprehensively verify the robust performance of the AAREMS for smart homes, Monte Carlo feasibility check is applied in this case study. In total, 1000 scenarios of the real-time PV power generation and at-will loads are randomly generated by the Monte Carlo sampling method. These scenarios follow the Gaussian probability distribution within the predicted intervals. The optimised smart home day-ahead

Table 3 Feasibility check results

Result	Minimum value	Maximum value
exchange power, kW	−1.425 (export)	4.000 (import)
BESS SOC, %	2.67	81.39
BESS O&M cost, $	0.1440	0.1683
total cost $	7.4205	7.4448

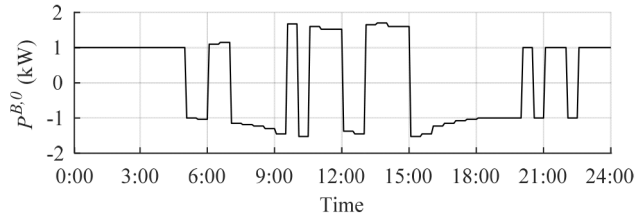

Fig. 11 *BESS base output power for cloudy day case*

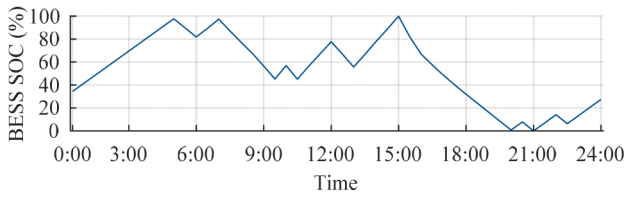

Fig. 12 *BESS SOC under the worst case for cloudy day case*

scheduling decision demonstrated in Section 6.2.1 is applied and the 1000 scenarios as the uncertainty realisation are given to the optimised affinely adjustable control of the BESS.

The BESS affinely adjustable control can achieve a certain and invariable power exchange result as the red curve shown in Fig. 10. This power exchange for all the uncertainty realisation scenarios is exactly the same as the optimised one in the day-ahead scheduling, which verifies the uncertainty sets can cover all the uncertainty realisation to achieve the certain and invariable power exchange.

For all the 1000 scenarios, the minimum and maximum values of the exchange power, BESS SOC, BESS O&M cost and total operating cost are analysed and shown in Table 3.

The power exchange between the smart home and the grid is kept within the allowed limit, 5 kW. Besides, the SOC does not reach the maximum or minimum limit, which indicates the BESS can always support sufficient energy capacity to charge/discharge power in real time. Thus, the AAREMS is robust against any uncertainty realisation without any operating constraint violation.

In terms of the operating costs, since the real-time BESS output power varies around the base output power frequently, the BESS O&M cost does not change much, and the total operating cost is achieved with a slight difference.

6.3 Simulation results of cloudy day case

6.3.1 Day-ahead scheduling decisions: Moreover, the AAREMS problem is solved for the cloudy day case. Since the PV power generation during the midday is low, the minimised objective under the worst case is increased to $13.8300.

The optimised BESS base output power and the BESS SOC under the worst case for the cloudy day case are demonstrated in Figs. 11 and 12, respectively.

During the midday, due to the lower PV power generation, the BESS charging power is lower than that under the sunny day case. For the same reason, the BESS stores more energy from the grid during the off-peak periods. Same with the sunny day case, the BESS in the cloudy day case discharges power when the deferrable loads are used.

Additionally, the optimised schedule of the deferrable loads is given in Table 4.

Under the cloudy day case, the morning appliances are scheduled during the morning off-peak period and the evening appliances are scheduled as early as possible to directly consume

Table 4 Optimally scheduled deferrable loads for cloudy day case

Deferrable load	Operation time	Deferrable load	Operation time
clothes washer	8:30–9:30	microwave oven	12:30–13:00
	12:00–13:00		15:00–15:30
clothes dryer	12:00–13:00		15:30–16:00
dishwasher	15:00–17:00		17:30–18:00
iron	5:00–6:00	rice cooker	14:30–15:30
vacuum cleaner	9:00–9:30	kettle	5:30–6:00
	10:00–10:30	toaster	5:00–5:30

Table 5 Feasibility check results for cloudy day case

Result	Minimum value	Maximum value
exchange power, kW	−0.875 (export)	3.037 (import)
BESS SOC, %	6.70	78.85
BESS O&M cost, $	0.1315	0.1565
total cost, $	9.8187	9.8436

the PV power generation, to minimise the grid electricity usage bill.

For the cloudy day case, the solver time is only 3.1528 s, also indicating high computing efficiency.

6.3.2 Monte Carlo feasibility check: The Monte Carlo feasibility check with 1000 randomly sampled scenarios of uncertainty realisation is also applied for the cloudy day case by testing the optimised affinely adjustable control. The optimised deferrable load tasks and BESS affine control function illustrated in Section 6.3.1 are applied.

Through the testing with the scenarios, the certain and invariable power exchange is achieved by the BESS affinely adjustable control for each uncertainty realisation scenario.

For all the 1000 scenarios, the analysis results of the feasibility check for the cloudy day case are given in Table 5.

It can be seen that for the cloudy day case, the power exchange and the BESS SOC are kept within the allowed limits, indicating operating robustness against any uncertainty realisation to guarantee all the operating constraints. Besides, the total operating cost which does not change much is less than the optimised one, since the worst-case does not occur.

7 Conclusions and future works

This paper proposes an AAREMS for smart homes which can robustly optimise the coordinated operation of the deferrable loads and the BESS affinely adjustable control under the uncertainties. Moreover, the AARC is applied to solve the AAREMS optimisation problem under the worst case of uncertainty realisation. The proposed AAREMS is simulated with a sunny day case and a cloudy day case, and the simulation results verify that the AAREMS can minimise the total operating cost efficiently with all the operating constraints satisfied. In addition, by the BESS affinely adjustable control, the power exchange is kept as the day-ahead optimised value without any fluctuation. Moreover, the proposed AAREMS is tested with 1000 Monte Carlo sampled scenarios to check the solution feasibility, i.e. the operating robustness. The results show no operating constraint violation and the power exchange is kept constant against any realised fluctuations. Thus, the proposed AAREMS can guarantee the operating robustness under the uncertainties.

In future works, building thermal models, multiple smart homes and their impacts on the distribution network as well as uncertainty budgets can be considered in the proposed AAREMS for smart homes.

8 Acknowledgments

This research was partially supported by the UNSW Digital Grid Futures Institute and the ARC Research Hub for Integrated Energy Storage Solutions (Project ID: IH180100020).

9 References

[1] Zhang, C., Xu, Y., Dong, Z.Y., *et al.*: 'Three-stage robust inverter-based voltage/var control for distribution networks with high-level PV', *IEEE Trans. Smart Grid*, 2019, **10**, (1), pp. 782–793

[2] Liu, L., Liu, Y., Wang, L., *et al.*: 'Economical and balanced energy usage in the smart home infrastructure: a tutorial and new results', *IEEE Trans. Emerging Top. Comput.*, 2015, **3**, (4), pp. 556–570

[3] Benefits of demand response in electricity markets and recommendations for achieving them. US Dept. Energy Tech. Report, 2006. Available at http://energy.gov/oe/downloads/benefits-demand-response-electricity-markets-and-recommendations-achieving-them-report

[4] Yaghmaee, M.H., Moghaddassian, M., Leon-Garcia, A.: 'Autonomous two-tier cloud-based demand side management approach with microgrid', *IEEE Trans. Ind. Inf.*, 2017, **13**, (3), pp. 1109–1120

[5] Nourai, A., Kogan, V.A., Schafer, C.M.: 'Load leveling reduces T&D line losses', *IEEE Trans. Power Del.*, 2008, **23**, (4), pp. 2168–2173

[6] Hannan, M.A., Faisal, M., Ker, P.J., *et al.*: 'Review of optimal methods and algorithms for sizing energy storage systems to achieve decarbonization in microgrid applications', *Renew. Sustain. Energy Rev.*, 2020, **131**, pp. 1–24

[7] Hoppmann, J., Volland, J., Schmidt, T.S., *et al.*: 'The economic viability of battery storage for residential solar photovoltaic systems - A review and a simulation model', *Renew. Sustain. Energy Rev.*, 2014, **39**, pp. 1101–1118

[8] Li, X., Hui, D., Lai, X.: 'Battery energy storage station (BESS)-based smoothing control of photovoltaic (PV) and wind power generation fluctuations', *IEEE Trans. Sustain. Energy*, 2013, **4**, (2), pp. 464–473

[9] Yao, E., Samadi, P., Wong, V.W.S., *et al.*: 'Residential demand side management under high penetration of rooftop photovoltaic units', *IEEE Trans. Smart Grid*, 2016, **7**, (3), pp. 1597–1608

[10] Wang, Y., Lin, X., Pedram, M.: 'A near-optimal model-based control algorithm for households equipped with residential photovoltaic power generation and energy storage systems', *IEEE Trans. Sustain. Energy*, 2016, **7**, (1), pp. 77–86

[11] Arun, S.L., Selvan, M.P.: 'Dynamic demand response in smart buildings using an intelligent residential load management system', *IET Gener. Transm. Distrib.*, 2017, **11**, (17), pp. 4348–4357

[12] Yang, J., Liu, J., Fang, A., *et al.*: 'Electricity scheduling strategy for home energy management system with renewable energy and battery storage: a case study', *IET Renew. Power Gener.*, 2018, **12**, (6), pp. 639–648

[13] Zhang, C., Xu, Y.: 'Hierarchically-coordinated voltage/VAR control for distribution networks using PV inverters', *IEEE Trans. Smart Grid*, 2020, **11**, (4), pp. 2942–2953

[14] Correa-Florez, C.A., Michiorri, A., Kariniotakis, G.: 'Robust optimization for day-ahead market participation of smart-home aggregators', *Appl. Energy*, 2018, **229**, pp. 433–445

[15] Danandeh, A., Zhao, L., Zeng, B.: 'Job scheduling with uncertain local generation in smart buildings: two-stage robust approach', *IEEE Trans. Smart Grid*, 2014, **5**, (5), pp. 2273–2282

[16] Alam, M.J.E., Muttaqi, K.M., Sutanto, D.: 'A novel approach for ramprate control of solar PV using energy storage to mitigate output fluctuations caused by cloud passing', *IEEE Trans. Energy Convers.*, 2014, **29**, (2), pp. 507–518

[17] Balamurugan, E., Venkatasubramanian, S.: 'Analysis of double moving average power smoothing methods for photovoltaic systems', *Int. Res. J. Eng. Technol.*, 2016, **3**, (2), pp. 1260–1262

[18] Nazaripouya, H., Chu, C., Pota, H.R., *et al.*: 'Battery energy storage system control for intermittency smoothing using an optimized two-stage filter', *IEEE Trans. Sustain. Energy*, 2018, **9**, (2), pp. 664–675

[19] Wang, Y., Lin, X., Pedram, M.: 'Adaptive control for energy storage systems in households with photovoltaic modules', *IEEE Trans. Power Syst.*, 2014, **5**, (2), pp. 992–1001

[20] Liu, H., Yang, Y., Wang, X., *et al.*: 'An enhanced dual droop control scheme for resilient active power sharing among paralleled two-stage converters', *IEEE Trans. Power Electron.*, 2017, **32**, (8), pp. 6091–6104

[21] Nistor, M., Antunes, C.H.: 'Integrated management of energy resources in residential buildings—a markovian approach', *IEEE Trans. Smart Grid*, 2018, **9**, (1), pp. 240–251

[22] Heo, S., Park, W., Lee, I.: 'Energy management based on communication of smart plugs and inverter for smart home systems'. Proc. 2017 Int. Conf. on Information and Communication Technology Convergence, Jeju, 2017

[23] Zhang, C., Xu, Y., Li, Z., *et al.*: 'Robustly coordinated operation of a multi-energy microgrid with flexible electric and thermal loads', *IEEE Trans. Smart Grid*, 2019, **10**, (3), pp. 2765–2775

[24] Wan, C., Xu, Z., Pinson, P., *et al.*: 'Probabilistic forecasting of wind power generation using extreme learning machine', *IEEE Trans. Power Syst.*, 2014, **29**, (3), pp. 1033–1044

[25] Zhang, C., Xu, Y., Dong, Z.Y.: 'Robustly coordinated operation of a multi-energy micro-grid in grid-connected and islanded modes under uncertainties', *IEEE Trans. Sustain. Energy*, 2020, **11**, (2), pp. 640–651

[26] Ben-Tal, A., Goryashko, A., Guslitzer, E., *et al.*: 'Adjustable robust solutions of uncertain linear programs', *Math. Program.*, 2004, **99**, (2), pp. 351–376

[27] An, Y., Zeng, B.: 'Exploring the modeling capacity of two-stage robust optimization: variants of robust unit commitment model', *IEEE Trans. Power Syst.*, 2015, **30**, (1), pp. 109–122

[28] GUROBI. Available at http://www.gurobi.com, accessed September 2018

[29] Redondo-Iglesias, E., Venet, P., Pelissier, S.: 'Global model for self-discharge and capacity fade in lithium-ion batteries based on the generalized eyring relationship', *IEEE Trans. Veh. Technol.*, 2018, **67**, (1), pp. 104–113
[30] Lofberg, J.: 'YALMIP: a toolbox for modeling and optimization in MATLAB'. Proc. IEEE Int. Symp. Computer-Aided Control System Design, New Orleans, LA, 2004

10 Appendix

The proposed AAREMS has the following compact matrix model of the optimisation problem, which is also given in Section 5.3:

$$\min_{\boldsymbol{x},\boldsymbol{y}} \boldsymbol{a}^{\mathrm{T}}\boldsymbol{x} \tag{45}$$

$$\text{s.t.} \quad \boldsymbol{y} = \boldsymbol{C}\boldsymbol{x} + \boldsymbol{D}\boldsymbol{u} \tag{46}$$

$$\boldsymbol{A}\boldsymbol{x} \le \boldsymbol{b} \tag{47}$$

$$\boldsymbol{A}_{\mathrm{eq}}\boldsymbol{x} = \boldsymbol{b}_{\mathrm{eq}} \tag{48}$$

$$\boldsymbol{E}\boldsymbol{x} + \boldsymbol{F}\boldsymbol{y} + \boldsymbol{G}\boldsymbol{u} \le \boldsymbol{h} \tag{49}$$

$$\boldsymbol{u} \in \left[\boldsymbol{u}^{\mathrm{l}}, \boldsymbol{u}^{\mathrm{u}}\right] \tag{50}$$

First, the vector of control, dependent and slack variables can be formed as

$$\boldsymbol{x} = \left[\boldsymbol{\alpha}^{\mathrm{T}}\ \boldsymbol{P}^{\mathrm{B},0\mathrm{T}}\ \boldsymbol{P}^{\mathrm{ch}\mathrm{T}}\ \boldsymbol{P}^{\mathrm{dis}\mathrm{T}}\ \boldsymbol{P}^{\mathrm{def}\mathrm{T}}\ \boldsymbol{P}^{\mathrm{sur}\mathrm{T}}\boldsymbol{E}^{\mathrm{T}}\ \mathbf{SOC}^{\mathrm{T}}\ \boldsymbol{\beta}^{\mathrm{T}}\ \boldsymbol{\delta}^{\mathrm{T}}\right]^{\mathrm{T}},$$

where the bold symbols present the sub-vectors of the control variables $\alpha_{i,j,t}$ and $P_t^{\mathrm{B},0}$, the dependent variables P_t^{ch}, P_t^{dis}, P_t^{def}, P_t^{sur}, E_t and SOC_t and the slack variables β_t and $\delta_{i,j,t}$; respectively. $(\boldsymbol{v})^{\mathrm{T}}$ means transposition of the specified vector $\boldsymbol{v}$. It is worth noting that different sequences of these sub-vectors can be applied without affecting the model efficiency. The affinely adjustable variable vector $\boldsymbol{y}$ is defined as $\boldsymbol{P}^{\mathrm{B}}$ which is the vector of P_t^{B}. In addition, the uncertainty variable vector can be constructed as

$$\boldsymbol{u} = \left[\Delta\boldsymbol{P}^{\mathrm{PV}\mathrm{T}}\ \Delta\boldsymbol{P}^{\mathrm{ULT}}\right]^{\mathrm{T}},$$

where $\Delta\boldsymbol{P}^{\mathrm{PV}}$ and $\Delta\boldsymbol{P}^{\mathbf{UL}}$ denote the sub-vectors of $\Delta\boldsymbol{P}_t^{\mathrm{PV}}$ and $\Delta\boldsymbol{P}_t^{\mathrm{UL}}$, respectively.

Second, the objective function (45) is formed by (22), (24) and (25). In detail, as the coefficients for P_t^{ch}, P_t^{dis}, P_t^{def} and P_t^{sur} during each operation period, $\mathrm{OM}\tau$, $\mathrm{OM}\tau$, $p_t^{\mathrm{buy}}\tau$ and $-p_t^{\mathrm{sell}}\tau$ form the vector $\boldsymbol{a}$ at the corresponding entries, as

$$\boldsymbol{a} = \left[\mathbf{0}^{\mathrm{T}}\ \mathbf{0}^{\mathrm{T}}\ (\mathrm{OM}\tau)^{\mathrm{T}}\ (\mathrm{OM}\tau)^{\mathrm{T}}\ \tau\boldsymbol{p}^{\mathrm{buyT}}\ (-\tau)\boldsymbol{p}^{\mathrm{sellT}}\mathbf{0}^{\mathrm{T}}\ \mathbf{0}^{\mathrm{T}}\ \mathbf{0}^{\mathrm{T}}\ \mathbf{0}^{\mathrm{T}}\right]^{\mathrm{T}}.$$

Herein $\mathbf{0}$ means a vector of zero, $(\mathrm{OM}\tau)$ denotes a vector whose all elements are OM\tau, $\boldsymbol{p}^{\mathbf{buy}}$ and $\boldsymbol{p}^{\mathbf{sell}}$ present the vectors of the electricity prices p_t^{buy} and p_t^{sell}, respectively. It is worth noting that the sequence of the sub-vectors in $\boldsymbol{a}$ must follow the sequence of the sub-vectors of variables in $\boldsymbol{x}$.

Third, by setting the parameters as the entries for the corresponding variables, constraints (46)–(49) can be formed.

Constraint (46) is formed by the BESS affine function (3). The entry for each $P_t^{\mathrm{B},0}$ to P_t^{B} in $\boldsymbol{C}$ is set as 1 while others are 0. The entry for each ΔP_t^{PV} to P_t^{B} in $\boldsymbol{D}$ is set as 1 and that for each ΔP_t^{UL} to P_t^{B} is set as −1, while others are 0.

The smart home inequality operating constraints (6a), (6b), (12), (16a)–(16c), (17), (23b), (23c) and (21) with (23a) substituting for P_t^{SH} make up the matrix constraint (47). For (6a), (6b), for each operation period t, a sub-matrix inequality constraint $\boldsymbol{A}_6\left[P_t^{\mathrm{ch}}\ P_t^{\mathrm{dis}}\ \beta_t\right]^{\mathrm{T}} \le \boldsymbol{b}_6$ is formed as follows:

$$\boldsymbol{A}_6 = \begin{bmatrix} 1 & 0 & -P^{\mathrm{ch,c}} \\ 0 & 1 & P^{\mathrm{dis,c}} \\ -1 & 0 & 0 \\ 0 & -1 & 0 \end{bmatrix}, \quad \boldsymbol{b}_6 = \begin{bmatrix} 0 \\ P^{\mathrm{dis,c}} \\ 0 \\ 0 \end{bmatrix}.$$

Similarly, $\boldsymbol{A}_{12}[\mathrm{SOC}_t]^{\mathrm{T}} \le \boldsymbol{b}_{12}$ is formed for (12) with

$$\boldsymbol{A}_{12} = \begin{bmatrix} 1 \\ -1 \end{bmatrix}, \quad \boldsymbol{b}_{12} = \begin{bmatrix} \mathrm{SOC}_t^{\max} \\ -\mathrm{SOC}_t^{\min} \end{bmatrix}.$$

$\boldsymbol{A}_{16\boldsymbol{ab}}\left[\alpha_{i,j,t}\ \alpha_{i,j,t-1}\ \delta_{i,j,t}\right]^{\mathrm{T}} \le \boldsymbol{b}_{16\boldsymbol{ab}}$ is generated for (16a) and (16b) with

$$\boldsymbol{A}_{16\boldsymbol{ab}} = \begin{bmatrix} 1 & -1 & -1 \\ -1 & 1 & -1 \end{bmatrix}, \quad \boldsymbol{b}_{16\boldsymbol{ab}} = \begin{bmatrix} 0 \\ 0 \end{bmatrix}.$$

$\boldsymbol{A}_{16\boldsymbol{c}}\left[\delta_{i,j,1}\ldots\ \delta_{i,j,T}\right]^{\mathrm{T}} \le \boldsymbol{b}_{16\boldsymbol{c}}$ is formulated for (16c) with

$$\boldsymbol{A}_{16\boldsymbol{c}} = [1 \quad \ldots \quad 1], \quad \boldsymbol{b}_{16\boldsymbol{c}} = [2].$$

$\boldsymbol{A}_{17}[\alpha_{i,1,t}\ldots\alpha_{i,J,t}]^{\mathrm{T}} \le \boldsymbol{b}_{17}$ is constructed for (17) with

$$\boldsymbol{A}_{17} = [1 \quad \ldots \quad 1], \quad \boldsymbol{b}_{17} = [1].$$

$\boldsymbol{A}_{23\boldsymbol{bc}}\left[P_t^{\mathrm{def}}\ P_t^{\mathrm{sur}}\right]^{\mathrm{T}} \le \boldsymbol{b}_{23\boldsymbol{bc}}$ is formulated for (23b) and (23c) with

$$\boldsymbol{A}_{23\boldsymbol{bc}} = \begin{bmatrix} -1 & 0 \\ 0 & -1 \end{bmatrix}, \quad \boldsymbol{b}_{23\boldsymbol{bc}} = \begin{bmatrix} 0 \\ 0 \end{bmatrix}.$$

With (23a) substituting for P_t^{SH}, $\boldsymbol{A}_{21}\left[P_t^{\mathrm{def}}\ P_t^{\mathrm{sur}}\right]^{\mathrm{T}} \le \boldsymbol{b}_{21}$ is generated for (21) with

$$\boldsymbol{A}_{21} = \begin{bmatrix} 1 & -1 \\ -1 & 1 \end{bmatrix}, \quad \boldsymbol{b}_{21} = \begin{bmatrix} P_t^{\mathrm{IM,max}} \\ P_t^{\mathrm{EX,max}} \end{bmatrix}.$$

According to the corresponding entries of variables in $\boldsymbol{x}$, the above sub-matrices $\boldsymbol{A}_{(.)}$ and sub-vectors $\boldsymbol{b}_{(.)}$ constitute $\boldsymbol{A}$ and $\boldsymbol{b}$ in (47).

The smart home equality constraints (10), (11) and (14) construct the matrix constraint (48). For (10), for each operation period t, $\boldsymbol{A}_{\mathbf{eq}10}\left[P_t^{\mathrm{ch}}\ P_t^{\mathrm{dis}}\ E_t\ E_{t-1}\right]^{\mathrm{T}} = \boldsymbol{b}_{\mathbf{eq}10}$ is generated with the following sub-matrix and sub-vector

$$\boldsymbol{A}_{\mathbf{eq}10} = \left[\eta^{\mathrm{ch}}\tau \quad -\tau/\eta^{\mathrm{dis}} \quad -1 \quad \left(1-\eta^{\mathrm{sd}}\right)\right], \quad \boldsymbol{b}_{\mathbf{eq}10} = 0.$$

Similarly, $\boldsymbol{A}_{\mathbf{eq}11}[E_t\ \mathrm{SOC}_t]^{\mathrm{T}} = \boldsymbol{b}_{\mathbf{eq}11}$ is formed for (11) with

$$\boldsymbol{A}_{\mathbf{eq}11} = \left[-1 \quad E^{\mathrm{c}}\right], \boldsymbol{b}_{\mathbf{eq}11} = 0.$$

$\boldsymbol{A}_{\mathbf{eq}14}\left[\alpha_{i,j,t}\ldots\ \alpha_{i,j,T}\right]^{\mathrm{T}} = \boldsymbol{b}_{\mathbf{eq}14}$ is constructed for (14) with

$$\boldsymbol{A}_{\mathbf{eq}14} = [1 \quad \ldots \quad 1], \quad \boldsymbol{b}_{\mathbf{eq}14} = \left[\mathrm{OT}_{i,j}\right].$$

According to the corresponding entries of variables in $\boldsymbol{x}$, the above sub-matrices $\boldsymbol{A}_{\mathbf{eq}(.)}$ and sub-vectors $\boldsymbol{b}_{\mathbf{eq}(.)}$ construct $\boldsymbol{A}_{\mathbf{eq}}$ and $\boldsymbol{b}_{\mathbf{eq}}$ in (48).

Moreover, the inequality constraints with the BESS affine output, (8) and (9) can be reformulated into a matrix form as $\boldsymbol{E}_{89}\left[P_t^{\mathrm{ch}}\ P_t^{\mathrm{dis}}\right]^{\mathrm{T}} + \boldsymbol{F}_{89}\left[P_t^{\mathrm{B}}\right]^{\mathrm{T}} \le \boldsymbol{h}_{89}$ with

$$\boldsymbol{E}_{89} = \begin{bmatrix} -1 & 0 \\ 0 & -1 \end{bmatrix}, \quad \boldsymbol{F}_{89} = \begin{bmatrix} 1 \\ -1 \end{bmatrix}, \quad \boldsymbol{h}_{89} = \begin{bmatrix} 0 \\ 0 \end{bmatrix}.$$

Further with the uncertainties, by substituting $P_{i,j,t}^{\mathrm{DL}}$ with (13), substituting P_t^{SH} with (23a), as well as substituting $\tilde{P}_t^{\mathrm{PV}}$ and $\tilde{P}_t^{\mathrm{UL}}$ with (18) and (19), constraints (4) and (20) can be reformulated as $\boldsymbol{E}_{420}\left[\alpha_{1,1,t}\ldots\ \alpha_{i,j,t}\ P_t^{\mathrm{def}}\ P_t^{\mathrm{sur}}\right]^{\mathrm{T}}+\boldsymbol{G}_{420}\left[\Delta P_t^{\mathrm{PV}}\ \Delta P_t^{\mathrm{UL}}\right]^{\mathrm{T}}\le\boldsymbol{h}_{420}$ with the following sub-matrices and sub-vector:

$$\boldsymbol{E}_{420}=\begin{bmatrix}-P_1^{\mathrm{DL,r}}\ldots & -P_i^{\mathrm{DL,r}} & 1 & -1\\ P_1^{\mathrm{DL,r}}\ldots & P_i^{\mathrm{DL,r}} & -1 & 1\end{bmatrix},$$

$$\boldsymbol{G}_{420}=\begin{bmatrix}1 & -1\\ -1 & 1\end{bmatrix},\quad \boldsymbol{h}_{420}=\begin{bmatrix}P^{\mathrm{ch,c}}+P_t^{\mathrm{BL}}+\bar{P}_t^{\mathrm{UL}}-\bar{P}_t^{\mathrm{PV}}\\ P^{\mathrm{dis,c}}-P_t^{\mathrm{BL}}-\bar{P}_t^{\mathrm{UL}}+\bar{P}_t^{\mathrm{PV}}\end{bmatrix}.$$

The above sub-matrices $\boldsymbol{E}_{89}$, $\boldsymbol{E}_{420}$, $\boldsymbol{G}_{420}$ and $\boldsymbol{F}_{89}$ and sub-vectors $\boldsymbol{h}_{89}$ and $\boldsymbol{h}_{420}$ form $\boldsymbol{E}$, $\boldsymbol{F}$, $\boldsymbol{G}$ and $\boldsymbol{h}$ in (49).

Last, (50) presents the uncertainty sets (28) and (29) in a form of vectors. The vector-based lower and upper bounds of the uncertainty sets are expressed as

$$\boldsymbol{u}^{\mathrm{l}}=\left[\left(\boldsymbol{P}^{\mathrm{PV,l}}-\bar{\boldsymbol{P}}^{\mathrm{PV}}\right)^{\mathrm{T}}\left(\boldsymbol{P}^{\mathrm{UL,l}}-\bar{\boldsymbol{P}}^{\mathrm{UL}}\right)^{\mathrm{T}}\right]^{\mathrm{T}},$$

$$\boldsymbol{u}^{\mathrm{u}}=\left[\left(\boldsymbol{P}^{\mathrm{PV,u}}-\bar{\boldsymbol{P}}^{\mathrm{PV}}\right)^{\mathrm{T}}\left(\boldsymbol{P}^{\mathrm{UL,u}}-\bar{\boldsymbol{P}}^{\mathrm{UL}}\right)^{\mathrm{T}}\right]^{\mathrm{T}},$$

where $\boldsymbol{P}^{\mathrm{PV,l}}$, $\boldsymbol{P}^{\mathrm{PV,u}}$, $\bar{\boldsymbol{P}}^{\mathrm{PV}}$, $\boldsymbol{P}^{\mathrm{UL,l}}$, $\boldsymbol{P}^{\mathrm{UL,u}}$ and $\bar{\boldsymbol{P}}^{\mathrm{UL}}$ present the sub-vectors of $P_t^{\mathrm{PV,l}}$, $P_t^{\mathrm{PV,u}}$, $\bar{P}_t^{\mathrm{PV}}$, $P_t^{\mathrm{UL,l}}$, $P_t^{\mathrm{UL,u}}$ and $\bar{P}_t^{\mathrm{UL}}$, respectively.

It is worth noting that the variables can be sorted in different sequences to form the variable vectors ($\boldsymbol{x}$, $\boldsymbol{y}$ and $\boldsymbol{u}$), then all the matrices and vectors of the parameters are formed accordingly. This appendix provides one example of the compact matrix construction method. Besides, the other matrices and vectors following the different variable sequences can be made up and applied without affecting the efficiency of the proposed AAREMS method.